calculation, the start current is usually reduced from the idealized value found under the assumption of perfect transmission there, although there are ranges of L for which interference between the coupled waves in the interaction region actually increases I_{st}. Because of the high Q nature of their resonators, start currents are generally lower in SWOs than in BWOs. Overall, start currents are increased when one takes account of the actual time dependence of I_b and γ_b, rather than assuming constant values for each.

For the finite values of the magnetic field, the behavior of I_{st} and device operation overall are modified significantly by the competition between the Cerenkov growth mechanism and absorption by spatial harmonics of the fast cyclotron wave.[44] The effect is most pronounced in the vicinity of the resonant magnetic field value, B_{res}, defined as the field at which the (−1)st spatial harmonic of the fast cyclotron wave resonates with the SWS at the same frequency as the Cerenkov resonance, so that the two compete. Thus, if ω_0 and k_{z0} are the values of frequency and wavenumber at the Cerenkov resonance between the SWS and the beam, then

$$\omega_0 \approx \left(k_{z0} - h_0\right)v_b + \Omega_c = \left(k_{z0} - h_0\right)v_b + \frac{eB_{res}}{m\gamma_b} \tag{8.11}$$

Since the Cerenkov resonance occurs where the beam line of Equation 8.6 is $n' = 0$, B_{res} is given by

$$B_{res} \approx \frac{2\pi m\gamma_b v_b}{ez_0} \tag{8.12}$$

The situation for magnetic fields at or near resonance is rather complicated, but generally I_{st} is increased, the stability of the interaction at larger currents is affected, and under some circumstances cyclotron absorption can make device operation impossible. Note also that resonances with higher-order spatial harmonics of the fast cyclotron frequency are possible, so that there are resonant field values at multiples of the value in Equation 8.12.

Although I_b must exceed I_{st} in order for an oscillator to operate, it is possible to have too much of a good thing. Levush et al.,[42] using a formalism and assumptions different from those of Swegle,[35] show that two nonlinear instabilities will modify, and in many cases degrade, the output behavior of a BWO for I_b appreciably above I_{st}. Figure 8.11 is a map of the regions of instability in a two-dimensional parameter space of dimensionless variables; the normalized length on the horizontal axis is the actual SWS length L divided by v_b/ω_0, with ω_0 the operating frequency, while the vertical axis is proportional to the length of the system and the beam current divided by the cube of $N = L/z_0$.* For the plot, the following parameters are fixed: (1) the

* The normalization parameter for I_b is rather complex, and in the interest of brevity, we refer the reader to Levush et al.[42] for details.

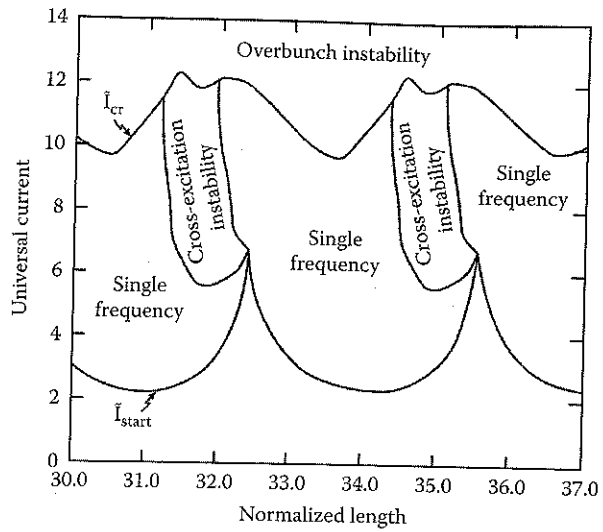

FIGURE 8.11
Regions of BWO operation in a space of normalized device current and normalized device length, assuming a combined reflection coefficient of 0.7 at the two ends of the device. (From Levush, B. et al., *IEEE Trans. Plasma Sci.*, 20, 263, 1992. With permission.)

product of magnitudes of the complex reflection coefficients at the ends, (2) v_b, and (3) the group velocity of the slow-wave-structure wave at resonance. Note that there are regions where one expects (1) single-frequency operation, (2) the *cross-excitation instability*, or (3) the *overbunch instability*.

The cross-excitation instability parameter space extends upward from the cusps in the lower boundary of the single-frequency region for values of $I_b > I_{st}$. On physical grounds, this happens because those cusps reflect rapid changes in I_{st} as the system shifts from one lowest-order axial mode to the next as the normalized length, $L\omega_0/v_b$, increases. This instability results from a nonlinear reduction in the start current for a competing axial mode in the vicinity of this region where axial modes shift. It manifests itself as shown in Figure 8.12, where the system begins oscillating in a lower-frequency mode, later jumping to a slightly *higher* frequency in a different axial mode; note that in a sense, system performance is improved by the higher-power operation in the latter mode. This instability has been observed experimentally.[45]

The overbunch instability, on the other hand, is a nonlinear effect resulting from the very strong beam bunching that occurs when I_b is substantially larger than I_{st}; this leads to operation in the primary mode as well as a sideband *downshifted* in frequency (similar to behavior observed in klystrons and other O-type sources). This sideband strongly modulates the output signal. Levush et al.[42] note that for much larger currents, with $I_b \sim 30I_{st}$, the microwave fields become so large that electron velocities are actually reversed.

As a rule of thumb, to avoid nonlinear instabilities that create mode hopping and sideband formation, it is desirable to operate an oscillator of this

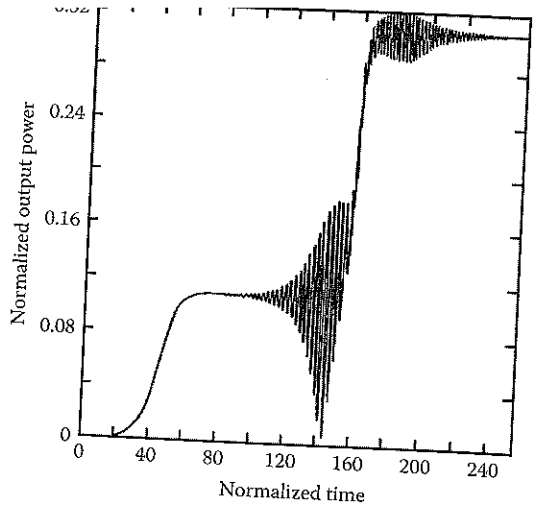

FIGURE 8.12
The behavior of the output power as a function of time when the cross-excitation instability sets in during BWO operation. (From Levush, B. et al., *IEEE Trans. Plasma Sci.*, 20, 263, 1992. With permission.)

type at I_b about three to five times I_{st}. Above about 30 times I_{st}, stochastic operation with broad spectral content results.

As we mentioned in the last section, the issue of start currents does not apply to amplifiers, since it is the goal of amplifier designers to prevent their device from breaking into oscillations. The important parameter for oscillators is the gain, defined as the ratio of output to input microwave power in Equation 8.10. At low-input power levels, G is roughly a constant that can be calculated approximately from the dispersion relation using a real value for ω (so that there is no temporal growth, which would make it an oscillator) to calculate the complex k_z. In the vicinity of a TWT beam–SWS resonance, for fields that vary as $\exp(ik_z z)$, the imaginary part of k_z, $\mathrm{Im}(k_z)$, will be negative, so that the field grows exponentially with length. Because the power is proportional to the square of the electric field, for small values of P_{in} and a SWS of length L,

$$G \approx \exp\left[2\left(\mathrm{Im}\, k_z\right)L\right] \tag{8.13}$$

As P_{in} is increased, P_{out} will begin to saturate, approaching some maximum value for a given beam current I_b, accelerating voltage and device efficiency.

8.3.4 Peak Output Power: The Role of Computer Simulation

There is no reliable analytic theory to compute the output power of an oscillator or the saturation power of an amplifier. To estimate these, and to optimize a device that is being built and tested, we turn to computer simulation. Before we consider the conversion of beam power to output microwave power, let us first consider the beam as the energy source to be tapped to make microwaves. We focus here on the current–voltage relationship for the beam, or more accurately, the relationship between current I_b and electron kinetic energy $(\gamma_b - 1)mc^2$, when it passes through the SWS. Remember from the discussion in Chapter 4 that space-charge effects from the beam will reduce γ_b from its value in the absence of space-charge forces, $\gamma_0 = 1 + eV_0/mc^2$, with V_0 the anode–cathode voltage in the beam diode. For a thin annular beam, γ_b is a function of γ_0, I_b, r_b, and the wall radius, which we approximate by the average radius r_0. Because the kinetic energy decreases as the current increases, the maximum power carried by the beam is a nonlinear function of these parameters; a useful expression for the maximum beam power is given in Vlasov et al.:[30]

$$P_{b,\max}\left(GW\right) = \frac{4.354}{\ln\left(r_0 / r_b\right)} W\left(\gamma_0\right)\gamma_0^2 \tag{8.14}$$

where the nonlinear function W(x) is plotted in Figure 8.13. Note that $P_{b,max}$ depends only on the anode–cathode voltage and the ratio of the wall and beam radii. As the beam approaches the wall, the maximum beam current becomes unlimited, although practically the beam–wall spacing is limited by the fact that with finite magnetic fields, one must allow enough spacing to limit the amount of beam current striking the wall (see Problem 7). As an aside, we note also that as the beam approaches the wall, sources with strong axial fields near the wall — SWOs and MWCGs, as well as RDGs operating near the Wood's anomalies discussed in conjunction with Figure 8.9 — will have stronger beam–field coupling because the axial field in those devices is strongest near the wall.

To understand how one uses Equation 8.14 in the context of a real problem, consider the following example. A reasonable device efficiency is about 20%. Thus, 5 GW of electron beam power is required to produce 1 GW of microwaves. We have a foil-less diode that delivers a beam for which the ratio r_0/r_b is 1.2. Using Equation 8.14 and the plot in Figure 8.13, we see that 5 GW of electron beam power can be delivered at just over 500 kV (or for γ_0 somewhat larger than about 2). If we ignore space-charge depression of the actual beam factor, $\gamma_b \approx \gamma_0$, in order to make a simple estimate, the beam current must be at least 10 kA in order for the beam power to be 5 GW (since $P_b \approx V_0 I_b$), so that the actual diode impedance, $Z = V_0/I_b$, will be approximately 50 Ω. Now remember that this 5 GW is the *maximum beam power* that can be delivered by a diode operating at this voltage. And let us suppose that we wish to design a BWO that operates at a diode impedance of 100 Ω. Then in this case, with $P_b \approx V_0 I_b = V_0^2 / Z$, the beam voltage must be about 707 kV. Both diodes deliver about the same 5 GW of beam power to the BWO. The difference between the approximately 500-kV, 50-Ω beam and the

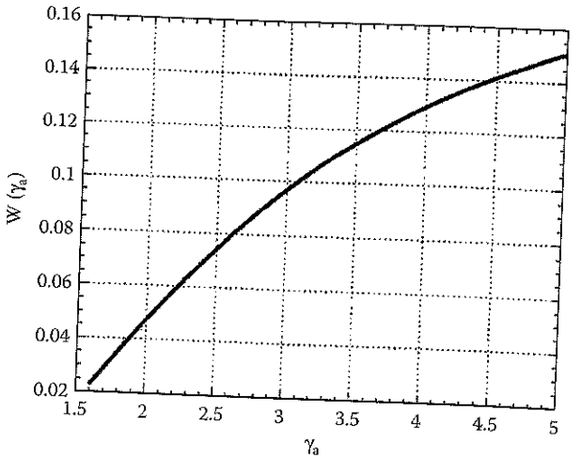

FIGURE 8.13
The function W in Equation 8.14. In the figure, we retain the original notation, with γ_a in the figure corresponding to γ_0 in our notation. (From Vlasov, A.N. et al., *IEEE Trans. Plasma Sci.*, 28, 550, 2000. With permission.)

707-kV, 100-Ω beam is that the former is optimized to deliver the maximum beam power possible at 500 kV, while the 707-kV beam is not optimized, in the sense that a higher beam power could be delivered at a lower impedance. That lower impedance, however, would not necessarily be the optimal impedance for the BWO itself.

Computer simulation with the 2-1/2-D MAGIC particle-in-cell (PIC) code shows the large-signal behavior of an overdriven BWO in Figure 8.14.[33] The output signal from a BWO with a sinusoidally rippled SWS is expressed in terms of a potential obtained by integrating the radial electric field component from the axis to the wall. The initial potential jump is an electrostatic effect due to the injection of the beam with a rise time of 0.2 nsec. The signal then grows exponentially in amplitude with a growth rate of about 1 nsec^{-1}, until growth saturates at about 7.5 nsec. Beyond that point, there is a strong amplitude modulation on the signal indicating the growth of a lower-frequency sideband such as would be created by the overbunch instability. The phase-space plot for the beam electrons given in Figure 8.15, plotted at about 10 nsec, shows the very strong effect of the microwave fields on the axial electron momenta. Near the entrance to the slow-wave structure, the axial momenta are strongly modulated, leading to bunching of the electrons. As the electrons move farther into the structure, the strong potential wells of the microwaves begin to trap some of the electrons, as we see from the large numbers of particles beyond about z = 15 cm that are bunched with small axial momenta. The fraction of the total population of electrons that are trapped trade energy back and forth with the waves with little net exchange, so that they modulate the microwave signal amplitude. Overall, at appreciable distances into the

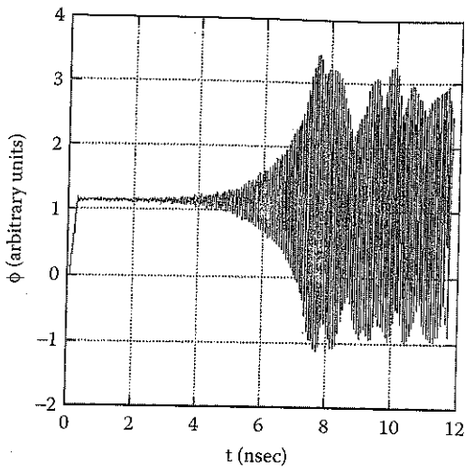

FIGURE 8.14
Time dependence of the signal calculated numerically for a BWO with an infinite axial magnetic field. The vertical axis is calculated by integrating the radial component of the microwave signal. (From Swegle, J.A. et al., *Phys. Fluids*, 28, 2882, 1985. With permission.)

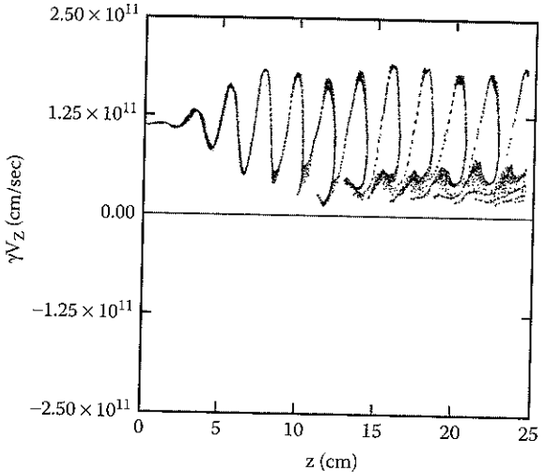

FIGURE 8.15
Phase-space plot of the electron momenta vs. position in a 25-cm-long SWS at t = 10 nsec in the device, with output as shown in Figure 8.14. (From Swegle, J.A. et al., *Phys. Fluids*, 28, 2882, 1985. With permission.)

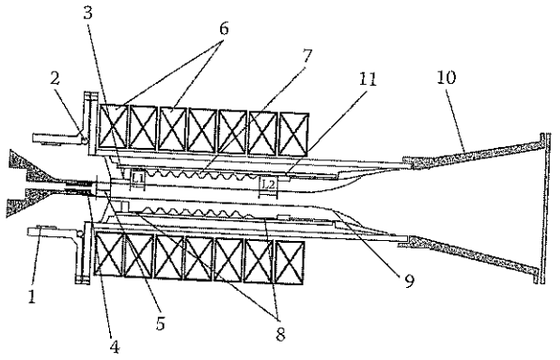

FIGURE 8.16
BWO at the University of New Mexico with both forward and backward shifting. (1) Capacitive voltage divider, (2) Rogowski coil, (3) cutoff neck, (4) cathode, (5) anode–cathode gap, (6) magnetic field coils, (7) slow-wave structure, (8) smooth circular waveguide and shifting lengths L_1 and L_2, (9) electron beam, (10) output horn antenna, and (11) reflection ring. (From Moreland, L.D. et al., *IEEE Trans. Plasma Sci.*, 24, 852, 1996. With permission.)

structure, there are more electrons with momenta less than the injection value at $z = 0$ than there are electrons with momenta over the injection value. Conservation of energy dictates that this energy has gone into the microwaves. The plots in Figure 8.14 and Figure 8.15 were made under the assumption of an infinite axial magnetic field; in other simulations with finite magnetic fields, the electrons moved radially as well, and some were lost to the walls of the slow-wave structure.

Computer simulations with the TWOQUICK PIC code were also used to investigate the effect of inserting smooth-walled drift sections before and after the SWS in a BWO, as shown in Figure 8.16.[17] When the length of the upstream section L_1 was varied from 0 to 40 mm, Figure 8.17 shows

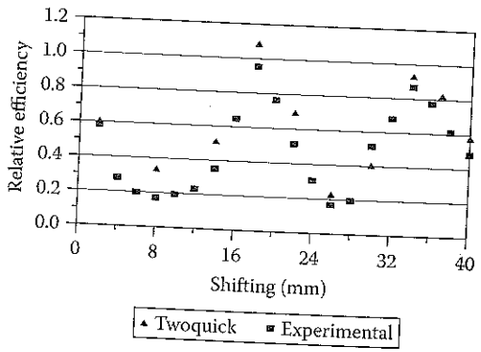

FIGURE 8.17
Variations in BWO power efficiency created by forward shifting with variations in the length L_1 in Figure 8.16. Results of both simulations with the TWOQUICK code and experiments are shown. (From Moreland, L.D. et al., *IEEE Trans. Plasma Sci.*, 24, 852, 1996. With permission.)

that the relative efficiency of microwave production varied by a factor of five in a periodic fashion. Although not shown, the frequency showed a similar variation, from about 9.7 GHz at 1 mm to 9.4 GHz at 6 mm to about 9.63 GHz at 17 mm. The simulations helped elucidate the role of the nonresonant space harmonic of the SWS mode in adjusting the phase between the beam current and the RF voltage to create the effects seen in the figure, effects that had also been considered elsewhere.[16,46] This technique has now become a standard for optimizing BWO output power and efficiency, as well as for providing mechanical tunability. A 670-MW X-band BWO operating at 25% power efficiency was built on the basis of this work, for example.

8.4 Operational Features

In this section, we consider the operational features for three different types of sources: (1) large-diameter multiwave devices, (2) much more compact BWOs, and (3) TWTs. The first two types represent two very different approaches to source construction. The ambitions of the former effort have been directed toward the maximization of peak power and energy per pulse over a very broad frequency range from 10 to 60 GHz, almost without regard to the volume and mass of the system. Much of the most important work was done on a mammoth test bed offering great, but not unlimited, flexibility in pursuing these ambitions. The latter has focused on a very different, but no less ambitious, set of goals: optimization of a multigigawatt BWO-based system in a compact package that operates repetitively and can be taken into the field. We compare some of the major results achieved for each system in Table 8.2. Finally, TWTs remain something of a work in progress, although they offer some unique features, such as an internal mode converter to get near-plane-wave output and the long-term possibility of master oscillator/power amplifier (MOPA) arrays that could offer high power without stressing any one source beyond its limits.

8.4.1 MWCGs, MWDGs, and RDGs

The peak power and frequency range over which gigawatt-level output power has been produced in the centimeter and millimeter regimes is very impressive: 15 GW at 9.4 GHz in an MWCG[12]; 0.5 to 1 GW at 17 GHz in an MWDG[10]; 3 GW at 31 GHz in an MWCG operating in a superradiant TWT-like mode[47]; and 3.5 GW at 46 GHz and 1 GW at 60 GHz in a two-section RDG.[14] In the series of shots that produced these last results, pulses of up to 700 nsec in duration were produced at somewhat lower power, and pulse energies of up to 350 J were radiated. The efficiencies claimed for these

TABLE 8.2

Comparison of Pulsed Power and Microwave Source Parameters for Representative Experiments Performed with MWCGs and RDGs Using the GAMMA Machine and with High Power BWOs on the SINUS Series of Pulsed Power Generators

E-Beam Generator	GAMMA	GAMMA	GAMMA	SINUS-6 (NAGIRA)	SINUS-6
Voltage	2.1 MV	1.2 MV	1.5 MV	600 kV	1 MV
Current	15 kA	12 kA	20 kA	5 kA	14 kA
Impedance	140 Ω	100 Ω	75 Ω	120 Ω	71 Ω
Pulse length	1 μsec	1 μsec	2.5 μsec	10 nsec (150-Hz repetition rate)	45 nsec
Slow-Wave Structure					
Diameter	14 cm	11.8 cm	11.8 cm		1.5 cm
Period	1.5 cm	4 mm	7 mm		1.61 cm
Total length					9.7 cm ($6z_0$)
Magnetic field	2.45 T		2.8 T		3.7 T
Source	**MWCG**	**MWCG**	**RDG**	**BWO**	**BWO**
Wavelength	3.15 cm	9.72 mm	6.5 mm	3 cm	3.2 cm
Power	15 GW	3 GW	2.8 GW	0.5 GW	3 GW
Duration	60–70 nsec	60–80 nsec	700 nsec	5 nsec	6 nsec
Pulse energy			520 J	2.5 J	20 J
Efficiency	48%	21%	9%	17%	21%

devices are equally impressive, peaking at a quoted value of 50% for the 15-GW MWCG*.

The test bed for many of the major achievements with these devices was GAMMA,[11] a large, Marx-driven, single-shot, pulsed power machine capable of producing 1-μsec voltage pulses when the output was crowbarred, and a pulse of up to 15-μsec duration in a rundown mode when the Marx capacitors just discharged through the diode and any leakage paths. Total electron beam energy ranged up to 140 kJ. It was 6.5 m tall with a footprint of 4.7 × 4.7 m². Figure 8.18 shows the outside of the microwave interaction region of roughly 1 m in length, with magnetic field coils wrapped around the slow-wave structure. The slow-wave structure itself has an inner diameter of about 15 cm, and the output window at the left is 120 cm in diameter. GAMMA has since been shut down, and subsequent experiments with MWCGs use the SINUS-7M machine,[48] a shorter-pulse, somewhat lower-voltage machine.

* In a number of instances, there is some ambiguity in the claims for output power; in these instances, the quoted value is for power leaving the source and entering the waveguide for transport to an antenna, while in others, the value is for actual power radiated. Obviously, achieving a high radiated power requires optimization of both source and antenna operation. In some experiments, antenna efficiencies of about 50%, below optimal, reduced the radiated power well below that produced in the source. Here, we do not attempt to resolve this ambiguity for every source, but rather notify the reader and assume that the quoted power levels would in any event be quite close to the value that would be radiated if the antenna performance were optimized.

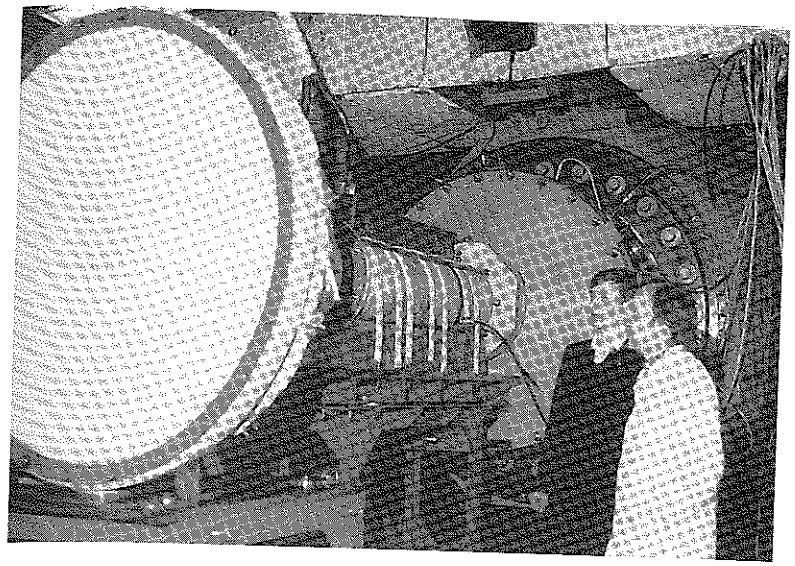

FIGURE 8.18
The microwave interaction region for HPM experiments conducted on the GAMMA machine at the Institute of High-Current Electronics in Tomsk, Russia. At the center, straps secure the magnetic field coils encircling the slow-wave structure. To the right of the interaction region lies the electron beam diode inside GAMMA. At the left of the picture is the window of the microwave horn radiator, behind which the beam electrons are collected on the walls of a flaring waveguide.

These devices use two (or more) slow-wave sections, separated by a drift space, each with a length roughly comparable to its diameter; in contrast to klystrons, the intervening drift space is not cut off and allows radiation to flow between sections. Examples are shown in Figure 8.19. Basically, the upstream section acts as a buncher, and the downstream section is an extraction section in which the bunched beam radiates; the driving beam current is insufficient to start oscillations in either section alone, but exceeds I_{st} for the aggregate. In the MWCG, each section operates in the π-mode (see Problem 8), like an SWO below its individual start condition, while in the MWDG, the upstream section operates in a backward wave mode and the downstream section operates in a $3\pi/2$ diffraction mode ($v_g \approx 0$). In RDGs, each section operates in the same, typically 2π, diffraction mode. These sources have large cross sections, with diameters D of up to 13 wavelengths in practice. The large diameter reduces the average power intensity and increases the overall power-handling capability of the slow-wave structure. The operating modes of the MWDG and RDG further reduce the fields at the walls because they are volume modes with field maxima closer to the axis (except in the case of those devices operating at the special Wood's anomalies).*

* Unfortunately, this point about mode patterns is beyond the scope of our treatment, since it involves an understanding of the details of the relative weighting of each spatial harmonic in the sum making up the expressions for the mode fields, but it is discussed in the MWDG and RDG references.

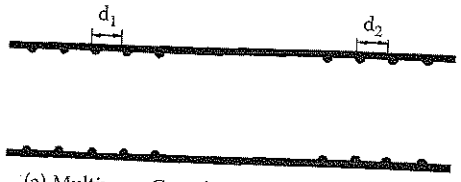

(a) Multiwave Cerenkov generator (MWCG)

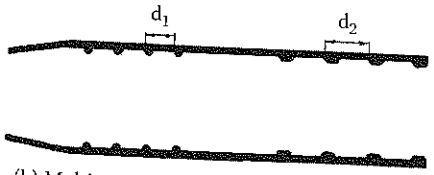

(b) Multiwave diffraction generator (MWDG)

FIGURE 8.19
Schematic of the walls of the cylindrical two-section slow-wave structures for an (a) MWCG (with $d_1 = d_2$) and (b) MWDG (or RDG). The electron beam enters from the left. The lengths of the two sections in each structure are, in general, different.

A recent review paper[48] discusses a detailed parameter study of the role of the structure parameters — length of each slow-wave section, length of the intermediate drift tube, and the ripple parameters — as well as the value of the magnetic field and the spacing between the annular beam and the wall, in optimizing MWCG performance on the SINUS-7M. Notably, the use of, and rationale for, three-section structures is discussed, as well as an apparent inverse proportionality between the optimum guiding magnetic field and beam spacing from the wall.

The large ratio of D/λ, however, makes mode control in these devices a challenge. The close spacing of the modes, the shortness of the slow-wave structures relative to their diameter, and the effect of the intense electron beam on the system dispersion characteristics make possible multiwave operation of modes all with the same frequency and similar values of k_z. Nevertheless, the mode control afforded by multiple sections results in a signal with a remarkably narrow spectral width. For example, the spectral width of a 9.4-GHz, 5-GW MWCG[49] with $D/\lambda \approx 5$ was 0.2 to 0.5%; at 35 GHz and 1. 5 GW, with $D/\lambda \approx 13$, the width was still only 0.5%,[47] which in this latter case was on the order of, or less than, the spacing between the normal modes of the slow-wave structure in the absence of the beam.

The experimentally observed increase in both peak power and pulse length with increasing D/λ is also remarkable. In a 9.4-GHz MWCG, when $D/\lambda \approx 3$, the output power and pulse length[50] were 5 GW and 30 to 50 nsec; increasing D/λ to 5 increased both power and pulse length to 15 GW and 60 to 70 nsec, while increasing efficiency as well. Further increases in D were prevented by the original geometry of the experiment, specifically the diameter of the solenoid providing the axial magnetic field, so subsequent MWCG experiments were performed at 31 and 35 GHz with the same D. At these higher frequencies and smaller values of λ, it was possible to demonstrate GW-level production for $D/\lambda = 13$. With these higher-frequency results in hand as a demonstration of mode control at this large value of D/λ, a series of initial experiments were performed with a larger, 38-cm-diameter structure.[51] At this larger diameter, GAMMA was capable of currents of 60 to 70 kA at voltages of 1.3 to 1.6 MV in 500- to 600-nsec pulses. Significantly, a 4-MJ Marx bank was needed to power the solenoidal field coil providing guide fields of up to 2.25 T. The system was shut down without optimizing the new configuration, however, and preliminary results of 3 GW in the X-band on an MWCG were unremarkable in themselves. We note that the operating beam impedance of almost 25 Ω is much less than the typical 100-Ω value for devices of this type. One other parameter that we shall discuss shortly, the linear beam current density, $I_b/2\pi r_b$, is about twice that for the 15-GW MWCG of Table 8.2, which had an efficiency of 48%, but comparable to that for the 2.8-GW MWCG with an efficiency of 9%.

The higher-frequency devices of Table 8.2 use quite small values of the wall period z_0. In Equation 8.12, we see that the resonant magnetic field for fast-cyclotron-wave effects scales as $1/z_0$. At higher frequencies it thus becomes difficult to operate at magnetic fields well above the resonant value, so that the field becomes a strong determinant of the operating frequency. In the RDGs of Bugaev et al.,[14] the magnetic field was a strong determinant of the frequency. Between 2.3 and 2.4 T, the output frequency was predominately in the 9- to 11.3-mm range, although there was considerable variation in the output frequency over the course of a pulse that extended over several hundred nanoseconds. At an intermediate field of 2.5 T, the output was unstable, with frequency content near 7.2 and 9 to 10 mm. At higher fields, between 2.6 and 2.8 T, the signal was concentrated in the 6.5- to 6.8-mm range. The longest pulse and greatest pulse energy were achieved with a field of 2.8 T, at a voltage of 1.5 MV and a current around 20 kA. At 46 GHz, 2.8 ± 0.8 GW in a 700-nsec pulse was generated, with a pulse energy of 520 J. Over the course of the microwave output pulse, the beam current rose and the voltage dropped continuously; we will return to this subject when we discuss pulse-length issues later in the next section.

The issues of beam control and pulse shortening are very important for these devices. Because these issues are still under investigation, and because they are of general interest, we cover them in Section 8.5.

8.4.2 BWOs

High power BWOs such as those used in the NAGIRA system are more compact and tend to operate for shorter pulses than the MWCG at power levels up to several gigawatts. Historically, the BWOs from the Institute of High-Current Electronics have been driven by electron beams generated with SINUS pulsed power machines, many times in a repetitively fired mode. A summary of SINUS machines is given in Table 8.3, which was compiled from a number of references.[52–58] The largest SINUS machine, the SINUS-7,

TABLE 8.3

Operating Parameters Quoted for High-Current, Pulse-Periodic Nanosecond Accelerators in the SINUS Family

	Voltage (kV)	Current (kA)	Pulse Length (nsec)	Pulse Energy (J)	PRR (pps)	Average Power (kW)	Reference
SINUS-200	350	3.5	3	3.7	1000	3.7	52
SINUS-M-3	220	0.7	3	0.5	1	0.0005	53
Not named	400	8	25	80	100	8	54
SINUS-4	500	3	30	45	50	2.3	55
SINUS-5	600	10	5	30	100	3	53
SINUS-6	700	7	20	98	100	9.8	56
SINUS-6L	800	8	25	160	1	0.2	53
SINUS-K	450	4.5	25	51	1000	51	52
SINUS-7	1500	50	50	3750	50	188	52
SINUS-700	1000	10	30	300	200	60	52
SINUS-8	200	15	20	60	400	24	53
SINUS-881	610	5.4	25	80	100	8	57
SINUS-13	200	7	7	9.8	100	1	58
SINUS-550-80	550	5	80	220	50	11	A.V. Gunin

is quite large, but the SINUS-500 and SINUS-6 are sized for field deployment in a complete system the size of a large shipping container. A SINUS-6 at the University of New Mexico is shown in Figure 8.20. More recently, a broader range of pulsed power machines has become available to drive these BWOs: an inductive storage machine from the Institute of Electrophysics in Ekaterinburg[59]; a modification of the SINUS generator with a spiral-wound pulse-forming line, which raises the impedance, to better match the impedance of the BWO, and shortens the system for a given pulse length[60]; and even a one-shot explosively driven generator.[61]

The NAGIRA system discussed in Chapter 2, which also uses a SINUS machine, has a number of interesting system features. First, the *impedance transformer* is a tapered transmission line that matches a 120-Ω BWO to the 20- to 50-Ω output impedance of the resonant Tesla transformer driving it. The length of the line is related to the length of the output pulse, and it evidently takes up a considerable fraction of the length of the container. Second, the BWO uses a superconducting magnet, a feature of systems like this since they appeared[62] in the late 1970s. As we will discuss in the next section, considerable effort has been devoted to reducing the magnetic field requirement for systems of this type. Third, the system uses quasi-optic transmission to the output dish.

BWOs of this type have produced gigawatt-level output in very compact microwave sources: 3 GW in an X-band device[63] and 5 GW in an S-band device.[64] Both were driven by a SINUS-7 machine: the X-band BWO with 1-MV, 14-kA pulses, and the S-band BWO with a 1.2-MV, 15-kA voltage and current pulse. The X-band BWO was fired repetitively, although it was limited to subhertz firing rates by the magnet of the BWO. The pulse-to-pulse standard deviation of output power was 3%. The output power was maximized by properly positioning the resonant reflector between the diode and the length of the slow-wave structure, a technique mentioned in Section 8.3.4 that was developed to optimize the phase relationship between the resonant backward space harmonic of the wave and the nonresonant forward space harmonic in the expansion of the fields.[16,17,46] We note that the resonant reflector used in these and other Russian BWO experiments differs from the solid reflector used in a number of other experiments.[17] The resonant reflector consists of a short section of the smooth-walled waveguide between the cathode and slow-wave section that has a significant step increase in radius. The optimized device length was actually quite short: $6z_0 = 9.7$ cm (three times the vacuum output wavelength), and it radiated a TM_{01}-like output mode. The 3-GW, 9.4-GHz pulses lasted 6 nsec, with about 20 J radiated per pulse. A plot of pulse length vs. output power is shown in Figure 8.21. The fit to the data indicates that the energy per pulse is apparently limited by pulse shortening to about 20 J, regardless of the output power. The authors note that at 3 GW, the peak wall fields in a smooth-wall waveguide are about 1.5 MV/cm, and previous work indicates that wall breakdown occurs in about 10 nsec for fields of 1 MV/cm.

The S-band device was referred to as a *resonance BWO*, because its operation depends on properly tailoring the interaction within the device by carefully choosing the length of the slow-wave structure and the length of

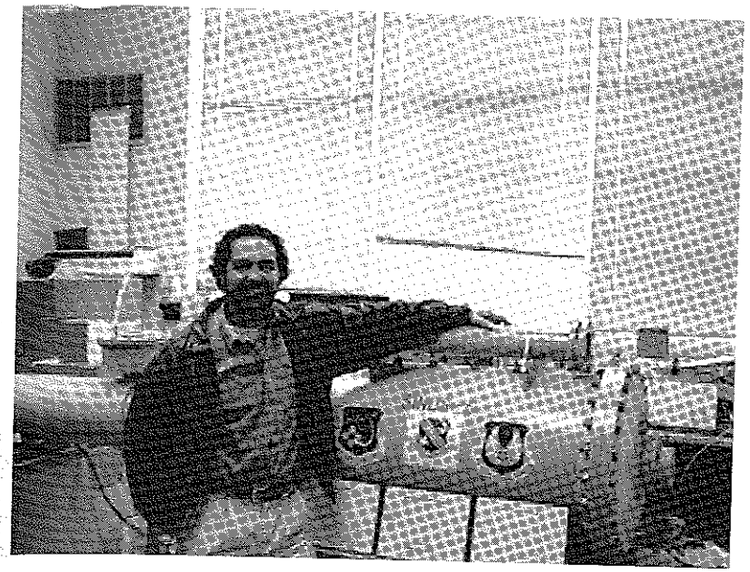

FIGURE 8.20
A SINUS-6 accelerator at the University of New Mexico in Albuquerque. The large section labelled "SINUS-6" is the integrated pulse-forming line and Tesla transformer; the cylindrical item on the top is used to trigger the gas switch between the pulse-forming line and the transmission line at the left of the figure.

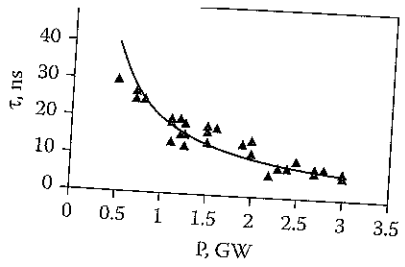

FIGURE 8.21
Microwave pulse duration vs. output power in a single-mode, 3-GW X-band BWO. (From Gunin, A.V. et al., *IEEE Trans. Plasma Sci.*, 26, 326, 1998. With permission.)

the smooth-walled section between the reflector at the beam input end and the slow-wave structure, as well as providing for additional wave reflection at the beam output end of the device. As a consequence, resonance BWOs can be made to be quite short; the SWS was only about 2.5λ, with λ the free-space wavelength of the radiated output, while the smooth-walled insert added about 0.7λ to the length. At peak output power of 5.3 GW, the efficiency of the device was about 30% and the pulse length was 25 nsec, with peak energy per shot around 100 J. Remarkably, the efficiency was rather constant as a function of electron beam power over the range between 5 and 19 GW of electron beam power. The mean diameter of the SWS for this S-band device was about one free-space wavelength.

One compromise route for balancing high output power and size is to increase the diameter of a single-section device, but to operate at a reduced voltage (which would reduce the size of the pulsed power). This approach was considered with a single-section 8.3-GHz SWO with D = 9.8 cm ($D/\lambda \sim 2.7$), which has been designed and tested[30] with the express purpose of achieving about 1 GW output at a voltage of 500 kV. Two estimates helped motivate the choice of a larger-diameter SWS:

- Using the expression for the maximum beam power at a given voltage (Equation 8.14), assuming a microwave generation efficiency of 20%, and requiring that the output power be 1 GW and the beam have a 5-mm standoff from the wall leads one to the estimate $D/\lambda \sim 2$.
- In a smooth-walled waveguide, the relationship between the power carried in a TM_{mp} mode P and the maximum field at the wall $E_{max,w}$ is (using our expression from Table 4.4)

$$P_{TM} = \frac{\pi r_0^2}{4Z_0}\left(1+\delta_{m,0}\right)\frac{E_{wall,\max}^2}{\left[1-\left(\frac{f_{co}}{f}\right)^2\right]^{1/2}} \tag{8.15}$$

where f_{co} is the cutoff frequency for the given mode and $\delta_{m,0} = 1$ if $m = 0$ and is zero otherwise.

Note that P scales as the area of the guide.

Having chosen D, the authors of Reference 30 considered several wall shapes (none of which was the sinusoidal wall of Equation 8.8), plotted the lowest-frequency dispersion relation for each, and then chose one that gave them an SWO. To enhance power, efficiency, and tunability, they used an upstream reflector with a movable smooth-walled-waveguide section. For details of the design process, refer to the reference. In experiments with this device, a peak output of 500 MW was achieved in a 10.2-J pulse with a 570-kV, 5.8-kA beam. The efficiency was about 15%, and a tunable range of about 120 MHz was achieved about the 8.3-GHz center frequency. Pulse shortening was observed at the highest power level; after several hundred shots, the middle section of the slow-wave structure was covered with damage spots. These spots were concentrated on the semicylindrical ends of the structure ripples, where peak fields exceeded 400 kV/cm.

8.4.3 TWTs

To restate a point made earlier, TWTs have received less attention than the high power Cerenkov oscillators. This may be because of the difficulty of controlling devices that are driven by such a powerful electron beam. As we will see, one of the two major efforts was plagued by sideband generation, while the other had trouble controlling oscillations. Here we concentrate on (1) a Cornell effort using solid "pencil" beams, rather than the more common annular beams, in a two-section, *severed* structure* (unlike the two-section MWDGs, for example, which allow propagation between sections) and (2) an effort involving the Institutes of High-Current Electronics in Tomsk and Applied Physics in Nizhny Novgorod, with collaboration from workers at the University of New Mexico, involving backward wave and traveling wave amplifiers operating in different azimuthal modes and coupled through a mode converter. We will also mention a Cornell effort that used a high power BWO to drive two TWTs in a master oscillator/power amplifier (MOPA) configuration.

The Cornell work using pencil beams in severed structures, which grew out of an effort that began with single-stage TWTs, is summarized in Shiffler et al.[65] In every case, the slow-wave structures had an average radius of 1.32 cm, a ripple depth of 8 mm, and a period of 7 mm, and operation was in the lowest TM_{01}-like mode. At each end, the ripple depth tapered to zero to minimize end reflections and the possibility of breaking into oscillation. Operation was in the X-band at a center frequency of 8.76 GHz. The electron

* A *sever* prevents propagation from one section to the next, typically absorbing microwaves as they attempt to pass.

had an energy of 850 kV, and the current could be varied from 800 to 1700 A. The single-stage devices had central sections of up to $22z_0$ in length, plus the tapered end regions. Maximum gains of 33 dB at output powers of 110 MW and efficiencies of 11% were achieved. At 70-MW output power, the phase of the output was locked to the phase of a 100-kW input magnetron with an accuracy of ±8°. Above 70 MW, sideband formation occurred, making phase control problematic. Bandwidth was quite narrow: 20 MHz at the 3-dB points on the gain curve.

The two-stage severed amplifier was adopted to prevent self-oscillations at high operating currents. Two amplifiers, each with center sections 22 ripples in length and tapers at the ends, were connected through a 9-mm-radius Poco graphite sever 13.6 cm long that attenuated the microwave signal by 30 dB, but allowed the space-charge waves on the beam to pass unattenuated to couple the two amplifier sections. The total signal output of about 400 MW, averaged over the pulse, was produced at an efficiency of 45%; gain was 37 dB. Bandwidth was considerably larger than that of the single-stage amplifier, of the order of 200 MHz. Unfortunately, sidebands were observed at all signal levels; at peak power, roughly half of the total power was in the sidebands. Computer simulations indicated that the bunching length in this system was quite long, and that the sideband development could be traced at least in part to finite-length effects and end reflections. Remarkably, even at instantaneous power levels up to 500 MW and pulse durations of about 70 nsec, no pulse shortening was observed.

The more complex amplifier from Tomsk, Nizhny Novgorod, and the University of New Mexico[24] produced substantially higher power using an 800-kV, 6-kA beam: up to 1.1 GW with a gain of 47 dB and an efficiency of 23%. The authors of this paper called out two challenging trade-offs in the design of HPM sources generally and HPM amplifiers specifically. First, to prevent breakdown, one must increase the cross-sectional dimensions of the source; however, in doing so, mode selection to produce a coherent output signal becomes more difficult. Second, high gain of the order of 40 to 50 dB is required if one wishes to use a conventional microwave source with power in the 10- to 100-kW range as the master oscillator. High gain, however, increases the chances that the source will break into self-oscillation, particularly under the relatively high noise conditions associated with relativistic electron beams. The authors' answer to these two challenges is the amplifier depicted in block diagram form in Figure 8.22 and schematically in Figure 8.23.

The input signal from a 100-kW, 9.1- to 9.6-GHz tunable magnetron is converted to a TE_{41} mode, which is preamplified in the backward wave amplifier. This amplifier — when run below its start oscillation condition — has a slow-wave structure with a corkscrew ripple like that shown in Figure 8.3d with azimuthal index $m' = 3$ on the ripple. Operating in the TE_{41} whispering-gallery mode, with index $m = 4$, the preamplifier produces a space-charge modulation on the beam with index $n = m - m' = 1$, which drives the downstream traveling wave tube in the HE_{11} hybrid mode. This mode is converted to a TE_{11} mode in the downstream waveguide and is radiated as a near-Gaussian beam from a horn antenna. The preamplifier has a mean diameter of 5.6 cm ($D/\lambda \sim 1.8$), while the mean diameter of the traveling wave amplifier is 6.46 cm. Axial magnetic fields up to 5 T could be applied. Gains in excess of 50 dB are possible, but over a narrow range of operating parameters. More desirably, lower gains of 43 to 44 dB can be achieved at comparable efficiencies of 35% or more and over a much wider range of operating parameters.

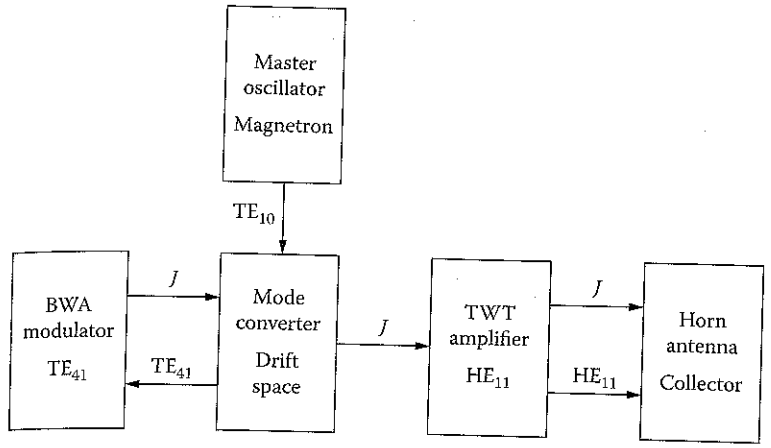

FIGURE 8.22
Block diagram of the 1.1-GW TWT amplifier developed by the Institute of Applied Physics in Nizhny Novgorod and the University of New Mexico. *J* indicates the direction of beam-current flow.

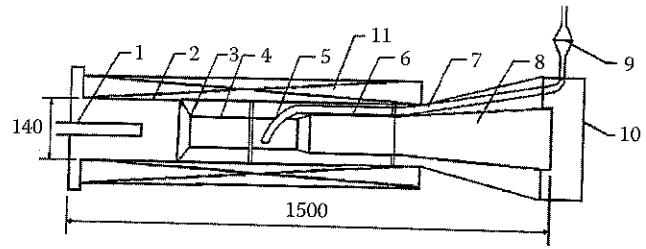

FIGURE 8.23
Schematic of the 1.1-GW TWT amplifier developed by the Institute of Applied Physics in Nizhny Novgorod and the University of New Mexico. (1) Cathode, (2) vacuum chamber wall, (3) matching horn, (4) backward wave amplifier modulator, (5) microwave input and drift space, (6) traveling wave amplifier, (7) input rectangular waveguide, (8) output horn, (9 and 10) input and output microwave windows, and (11) magnetic field-producing solenoid. Scale is in millimeters. (From Abubakirov, E.B. et al., *IEEE Trans. Plasma Sci.*, 30, 1041, 2002. With permission.)

The system can be run with the backward wave tube either above its oscillation threshold, in which event an output is produced without input from the conventional magnetron, or below it, so that an input is required to realize an output. The parameter governing the transition to self-oscillation in the backward wave tube is the radius of the electron beam; given a particular beam current and voltage, there is a minimum beam radius for

oscillation. For beam radii below that value, there are no oscillations; above that value, the backward wave tube goes into oscillation because the strength of the coupling between the beam and the structure reaches a requisite magnitude. A complication in the system is that the beam radius expands with a radial velocity of 1 to 2 cm/μsec over the course of the 500-nsec electron beam pulse. Thus, even when the system begins operation as an amplifier, it will transition to an oscillator when the beam radius expands outward through the threshold radius. When the backward wave tube is allowed to oscillate, the usual cyclotron resonance dip for these circularly polarized systems is seen in the vicinity of about 1.2 T. Higher-output powers, about 1.3 GW, were produced at fields above the dip, although power levels of about 1 GW were seen over a narrow range of fields below the dip. Given the polarization of the system, the polarity as well as the strength of the magnetic field affected performance. (Note: The estimate of the field at which the dip occurs, given in Equation 8.12, does not hold for these polarizations because the estimate does not take account of helically polarized waves.)

When run as an amplifier, the system achieves gains of 47 dB in a bandwidth of about 1% near the resonant frequency of the backward wave tube. Up to a 5% bandwidth could be reached through a coordinated tuning of the magnetic field and the beam radius. Pulse shortening is observed — the pulse length is 250 nsec at 300 MW (75 J, beam radius of 2 cm) and 70 nsec at 1.1 GW (77 J, beam radius of 2.1 cm) — but the authors offer that the benefits of increasing the device diameter have yet to be fully exploited.

Finally, a series of Cornell experiments examined the prototypical master oscillator/power amplifier (MOPA) configuration shown in Figure 8.24[25]

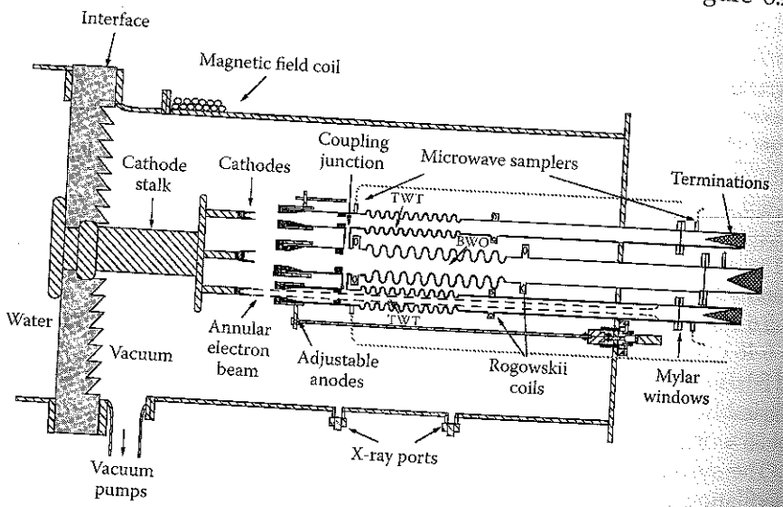

FIGURE 8.24
Layout of the Cornell master oscillator/power amplifier experiment. (From Butler, J.M. and Wharton, C.B., *Proc. SPIE*, 1226, 23, 1990. With permission.)

involving a relativistic BWO driving two relativistic TWTs. Unfortunately, a number of technical problems prevented the system from successful realization, but we discuss the configuration to illustrate the concept. Three cathodes energized by a single pulsed power unit were to provide three beams for a BWO and two TWTs; the BWO was to be the master oscillator for the two TWT amplifiers. The important feature of this arrangement was that it was to take advantage of the fact that pulsed power systems are capable of high-voltage operation at much lower impedances than those of individual BWOs and TWTs, which are typically about 100 Ω (although we note that the Cornell pencil-beam TWT was an order of magnitude higher in impedance). Two TWTs were coupled to a BWO at the upstream coupling junctions with rectangular waveguide sections. The TM_{01}-like mode of the BWO was converted to a rectangular-guide TE_{10} mode, and then reconverted to a TM_{01}-like mode of the TWTs.

8.5 Research and Development Issues

This is a relatively mature class of devices, but there are three major areas of research and development: (1) pulse shortening, which is a affliction for all HPM sources to one degree or another; (2) operation at lower magnetic fields, below the cyclotron-resonant field value, with a long-term goal of using lower-power direct current (DC) electromagnets or even permanent magnets; and (3) axially varying the SWS in order to raise device efficiency.

Beyond those three topics, there is the additional issue of the less mature sources in this class that deserve at least mention: the DCM, PCM, and even plasma-filled BWOs. We will mention these at the end. TWTs are also a less mature source, and in that regard, they qualify as an R&D issue, but we have already discussed the major research in this area.

8.5.1 Pulse Shortening

Pulse shortening involves a suite of factors: (1) breakdown in the power feed to the electron beam diode; (2) plasma motion in the diode that either closes the anode–cathode gap or causes the electron beam radius to increase with time; (3) breakdown processes in the SWS; and (4) beam stability issues within the SWS that cause anomalous electron beam loss. Three issues we will not consider here are plasma formation processes in the beam collector that leak plasma into the SWS; breakdown in the waveguide carrying microwaves away from the source; and breakdown in the antenna under the stress of extremely high power.

Breakdown in power feeds is an occupational hazard in the pulsed power business. One more subtle form of breakdown that caused early problems

in some experiments involved parasitic current flow from the cathode, or cathode feed, of the foil-less diode that creates the beam to the opposite wall of the transmission line, which sits at the anode potential.[66] This problem was solved rather straightforwardly by shaping the magnetic field near the electron-emitting surface so that the field lines intercepted a shield on the cathode side designed to catch electrons before they could leak across to the anode side of the feed or transmission line.

Plasma motion in the diode and the effect that it has on gap closure and beam radius growth are more difficult. The electron beam is generated by a process of explosive emission that creates a plasma at the emitting surface from which the beam is drawn. This plasma is confined by an axial magnetic field, and it can expand across the magnetic field, causing beam radius growth, or forward along the magnetic field toward the anode, causing gap closure. When the beam radius grows and the beam approaches the wall, the beam–SWS coupling changes. In the case of the TWT of Abubakirov et al.,[24] the increased coupling raised the gain to the point that the system broke into oscillation and could no longer effectively amplify the input signal. In oscillators, the increased coupling can reduce I_{st}, so that the ratio I_b/I_{st} grows to the point that one of the nonlinear modulational instabilities — the cross-excitation or overbunch instability — becomes a problem. Finally, the increase in r_b can cause the beam to intercept the input iris to the slow-wave structure, exacerbating gap closure problems and causing beam termination. Experiments have shown that cross-field expansion is exacerbated by the penetration of microwave fields into the anode–cathode region.[67]

Two basic approaches have been taken to reduce cross-field expansion. One method was to increase the magnetic field strength as a function of time, in order to hold the plasma in place as it diffused across the field; in effect, these researchers "brought the field to the plasma."[67] Another approach has been to reduce the density of the plasma at the cathode. In this regard, a multipoint cathode consisting of an array of resistor-ballasted carbon fibers was used to reduce the overall plasma density well below that created at the surface of standard annular "cookie cutter" cathodes.[68] Consequently, the cathode plasma density was reduced by two to three orders of magnitude, and an 8-μsec pulse was produced, albeit at the low power of 10 MW. Another means of reducing the plasma density is the use of disk, rather than cookie cutter, cathodes.[69]

Breakdown in the slow-wave structure is evidenced by damage marks on the SWS, and it has received a great deal of attention. In an extensive review of the problem,[70] the emission of plasmas from the wall, and the ambipolar diffusion driven by ions in that plasma, were identified as a primary cause of pulse shortening. Explosive emission is at least one source of the wall plasma, as indicated by the observation of pits on the wall suggestive of this process. Another is adsorbed gases on the slow-wave-structure wall. To reduce this latter effect, the slow-wave structure of a 3-GW, X-band BWO was electrochemically polished and liquid nitrogen traps were added to the vacuum system. As a result, the microwave pulse length was increased from 6 to 26 nsec, and the energy per pulse grew from 20 to about 80 J.

In computer simulations, electrons alone reduced the output power, but did not terminate the pulse. When ions were emitted, however, the output power became strongly dependent on the current density of electron emission from the walls, and above a certain electron current density, microwave emission ceased. The location of the plasma emission was significant: the closer the release of the plasma to the input end of a BWO, the more it affected the microwave output. Plasma at the input end, perhaps due in part to beam interception by the input iris, was most damaging. Thus, BWOs in which the efficiency and power are optimized by adjusting the location of the input-end reflector are most susceptible to this effect.

Additional confirmation for the processes described in Korovin et al.[70] might be drawn from the RDG work of Bugaev et al.[14] There, diagnostics showed that the current received at the output end of these devices grew with time. Further, x-ray diagnostics revealed that the additional current, beyond that of the electron beam, consisted of low-energy electrons carrying as much or more current than the beam by the end of the beam pulse.

During the production of very high power microwaves in the MWCG experiments producing X-band radiation at the level of 10 GW or more, beam transport during the microwave pulse was clearly seen to terminate.[71] This termination occurred despite the fact that a beam of the same current and voltage propagated through a smooth-wall structure of the same radius with the same guide field when no microwaves were generated. Striated damage patterns were observed on the slow-wave-structure walls. It was postulated that the beam broke into filaments and that $\mathbf{E} \times \mathbf{B}$ drifts involving the microwave fields drove these filaments to the wall; however, this phenomenon is still not clearly understood.

Increasing the diameter of the slow-wave structure clearly helps in one regard: Equation 8.15 shows that the maximum electric field at the wall for fixed microwave power drops as $(D/\lambda)^{-2}$. With regard to that field, we note that the maximum fields at the walls of the 3-GW BWO were approximately 1.5 MV/cm. There was also an indication, on the basis of rather limited data from the MWCG experiments, that lower values of the linear beam current density, $I_b/\pi D$, are more desirable than higher values, and there may even be an optimal value.[13] The value in the 15-GW experiment was about 0.35 kA/cm. This is an area where more research is needed.

8.5.2 BWO Operation at Lower Magnetic Fields

A plot of output power and pulse length as a function of magnetic field in the 3-GW BWO is shown in Figure 8.25.[63] The drop in power around 2 T results from the cyclotron resonance dip at the field given in Equation 8.12. Output power peaks around 3.7 T, and from the standpoint of output power or pulse length, there is no advantage to increasing the magnetic field above

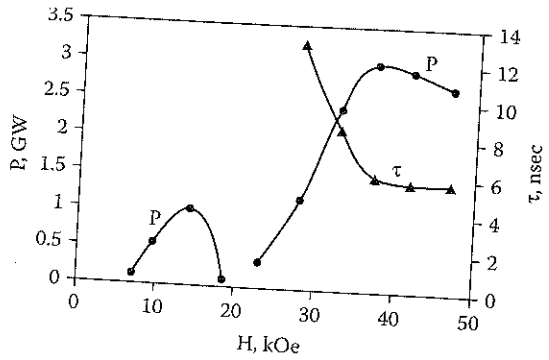

FIGURE 8.25
Microwave power and pulse duration for a single-mode, 3-GW X-band BWO. (From Gunin, A.V. et al., *IEEE Trans. Plasma Sci.*, 26, 326, 1998. With permission.)

that value. Below the cyclotron resonance, we see a local maximum in output power around 1.4 T, although the output power is lower there than it is at 3.7 T. Experiments with a larger-diameter SWS and beam, but a less powerful electron beam, produced 800 MW of output at 24% efficiency; this was intended to reduce the wall fields and show the way toward higher power and energy per pulse. In that larger-diameter device, though, we also note that comparable power was produced at magnetic fields below the resonance.

The use of a larger-diameter SWS and beam is important because beam quality and confinement are also issues below the cyclotron resonance. Preliminary experiments with a 10-GHz BWO showed that 500 MW of output could be produced in a device with a field of 0.7 T near the beam diode and 0.5 T inside the SWS. The DC field coil producing this field consumed 20 kW. At the larger radius, this device required more care in the selection of a TM_{01}-like operating mode.[72]

8.5.3 Axially Varying Slow-Wave Structures to Enhance Efficiency

Axially varying the interaction between the beam and the field as the beam loses energy to the field is a technique applied to increase efficiency in a number of microwave source types. Axial variations can involve modifying the coupling[73] or the phase velocity of the wave.[15] In the former case, a sinusoidally rippled slow-wave structure of total length L had relatively shallow ripples over a length L_{min}, followed by deeper ripples over the remainder. In the portion of the structure with deeper ripples, the magnetic field was decreased to allow the beam to approach the wall. By optimizing this configuration, the microwave generation efficiency was almost tripled, from 11% without the variations to 29% with them, resulting in an output power of 320 MW. In the latter case of varying the phase velocity, a 500-MW pulse was generated at 45% efficiency.

8.5.4 Other O-Type Sources: DCMs, PCMs, and Plasma-Filled BWOs

Dielectric Cerenkov masers (DCMs) and plasma Cerenkov masers (PCMs) operate in smooth-walled waveguides and use different slow-wave structures. In the DCM, slow waves are realized by using either a dielectric liner or rod within a smooth-walled waveguide. The material of the rod or liner is chosen for its high permittivity (or index of refraction), and the slower light speed in the material brings the dispersion curve for this slow-wave structure down below the speed of light; Equation 8.4 is modified to

$$\omega^2 = k_n^2 \bar{c}^2 + \bar{\omega}_{co}^2 (0, p) \tag{8.16}$$

In this equation, $\bar{c} < c$ because of the presence of the dielectric, and the cutoff frequency in Equation 8.5 has been modified to a value dependent on the modified speed of light. Beam–SWS resonances are possible, typically at high frequencies and wavenumbers (see Problem 10). Power levels in excess of 500 MW have been produced, as discussed in Section 8.2.

Plasma Cerenkov masers use plasma layers and the dispersion properties of the plasma to create slow-wave structures. Once again, a smooth-walled waveguide is used, and a low-energy electron beam (low energy by the standards of pulsed power) is used to create an annular plasma surrounding a high-energy electron beam, or perhaps a thin plasma rod on axis. Power levels of several hundred megawatts have been produced in PCMs, as indicated in Section 8.2.

The filling of BWOs with plasma to increase the allowable electron beam current within the SWS is an approach that traces back almost to the genesis of HPM.[74] The motivation for doing so is that the plasma provides space-charge neutralization of the beam, permitting one to use currents above the space-charge-limiting value for the vacuum SWS. Further, it is hoped that the neutralized beam will have higher quality than the beam in the vacuum SWS. In the initial high-current device, 600 MW of microwaves was generated, but only at 6 to 7% efficiency. A much higher efficiency of 40% was achieved in later work at 400 MW.[75] In the *pasotron* concept (plasma-assisted slow-wave oscillator, which was proven out at only tens of megawatts), the axial guide field was eliminated on the grounds that space-charge neutralization by the plasma would prevent radial expansion of the electron beam.[76]

8.6 Fundamental Limitations

Over the years, a number of groups have developed a substantial understanding of sources of this type. The values of output power, energy per pulse, and efficiency achieved within this group rank among the highest for

all HPM sources, and they have produced gigawatt power levels across a remarkable range in frequency, from 3 to 60 GHz. That range could be extended downward to begin to compete with magnetrons, which dominate in the L- and S-bands, although size could become an issue as the operating frequency is reduced. In magnetrons, the lowest passband extends upward in frequency from zero to the π-mode frequency. In the O-type Cerenkov devices, from Figure 8.6 and Equations 8.4 and 8.5, we see that the lowest passband extends upward from a minimum frequency $f \approx 11.5/r_0$, with f and r_0 measured in gigahertz and centimeters, respectively. We also know that the upper end of the passband for the lowest-order mode depends on the periodicity of the slow-wave structure, and that increasing z_0 lowers the frequency of the top of the passband. Thus, as the frequency goes down, device size grows both radially and axially.

The limitations in power, energy per pulse, and efficiency are actually of two classes: *absolute* and *system constrained*. Absolute limitations are the intrinsic limits set by the physics or the state of the technology in the absence of constraints on, for example, size or volume or electrical power consumption. System-constrained limitations, on the other hand, are those imposed by specific mission requirements, such as the demand for a mobile system or for a system with limited electrical demand. In the case of the absolute limits for these devices, we outline the pros and cons of the two major development thrusts in Table 8.4: (1) increasing D/λ to raise power, energy per pulse, and beam-to-microwave conversion efficiency and (2) operating at lower magnetic fields to reduce size, mass, electrical power demands, and temporal operating constraints imposed by pulsed, high-field magnets.

Increasing D/λ should improve the performance of the smaller gigawatt-level BWOs. Increasing the performance of the larger multiwave devices, however, begins to push the limit of ultimate device performance. Experiments on the GAMMA machine demonstrated the ability to operate at values as high as $D/\lambda = 13$. An X-band MWCG at this parameter value would have a slow-wave-structure diameter of about 40 cm. Adding magnetic field coils pushes the system diameter toward a meter. The mass of this magnet will become a major contribution to overall system mass, and the energy storage requirement for the magnet's power supply will grow as D^2, provided the length can be kept constant. These factors are examples of limitations potentially imposed by system constraints. If indeed the empirical observation of an optimal linear current density, $I_b/2\pi r_b$, in the range of 0.3 to 0.5 kA/cm holds — and the data are sufficiently limited that this is considered an issue to be resolved — then the optimum operating current might increase with D, and the operating impedance would drop as 1/D, if the voltage could be held constant, another uncertainty. Lower impedance either raises overall system efficiency as the source is brought into a better impedance match with the pulsed power or decreases system length if a tapered-line transformer matching the pulsed power and source impedances can be eliminated (see Problem 9). Increasing the operating current also increases the problem associated with the nonlinear cross-excitation and overbunching instabilities, which scale with the ratio I_b/I_{st}, and it will be necessary to design devices with higher start currents, which involves such measures as shortening the slow-wave structure or splitting it into multiple segments, to avoid those instabilities.

TABLE 8.4

Pros and Cons of the Two Main Approaches to Dealing with Device Limitations

Development Area	Pros	Cons
Increase D/λ	Reduce wall fields and lessen the probability of breakdown	Mode control
	Lower impedance, both to reduce voltage required to get requisite beam power and to better match source impedance to pulsed power	Existence of optimum linear beam current density, $I_b/2\pi r_b$, not fully explored
	Lower I_b relative to space-charge-limiting value and improve beam quality and confinement	Beam control issues not fully understood
		Start current must be pushed upward to avoid nonlinear instabilities at high current
Reduce B	Reduce electrical demand for electromagnets	Beam control
	Reduce mass and volume of magnets, including structural support	Output power is optimum only over a narrow range in B
	Make use of nonsuperconducting DC magnets possible	
	Eliminate temporal constraints mandated by the use of pulsed, high-field magnets	

Decreasing the operating magnetic field addresses a number of system constraints, but at the expense of raising additional issues in beam control. Because many systems use either a superconducting magnet for continuous operation — a system complication — or a long-pulse conventional magnet that limits the number of pulses that can be fired before the magnet pulse terminates, cutting the magnetic field is very desirable.

The role of the beam in pulse shortening is still not fully understood. The use of explosive emission cathodes is a foundation technology for these devices, since these cathodes are necessary to provide the multikiloampere currents that are required. The motion of the cathode plasma is a serious problem, however. Diode shorting and the growth of the beam radius may provide intrinsic limitations on pulse length and, as we saw, the ability to make operational TWTs with substantial energies per pulse. Once the beam enters the slow-wave structure, the underlying causes for the loss of the beam to the wall still need to be better understood before this limitation can be fully addressed.

Ultimately, device powers in unconstrained systems could be pushed into the tens of gigawatts if there is a demand for a system with the associated

size, mass, and electrical power demand. Alternatively, one could build compact, more highly optimized BWO-based systems, with longer pulses at current output power levels of several, to perhaps 10 or so, gigawatts, or smaller MWCG-based systems offering similar performance. The limited work in TWTs points to some possible advantages in pulse length, given the lower internal fields in amplifiers, as well as provides a more desirable output mode, but their lower level of development presents more uncertainties.

8.7 Summary

O-type Cerenkov devices are among the most versatile of HPM sources, with gigawatt power levels demonstrated between 3 and 60 GHz, and possibly down into the L-band if that were desired. Further, they have been operated repetitively when driven by the SINUS series of pulsed power machines, which can provide pulse rates up to 1000 Hz. In this repetitive mode of operation, a major consideration is the coil producing the guide magnetic field. Fields are sufficiently high that superconducting coils are used for operation over any appreciable time period.

The pursuit of high power operation has taken two directions, one involving large-diameter multisection slow-wave structures that operate in a multiwave mode (MWCGs, MWDGs, and RDGs) and another involving highly optimized BWOs of much smaller size. Overall, it is recognized that larger-diameter systems are required to achieve both high power and high energies per pulse. This places a burden on the designer to control the output mode of the device. Multiple paths, including multiwave operation, Bragg reflectors, and multisection devices with internal mode converters, are all being pursued in this regard. Ultimately, the power of these devices is limited more by overall system constraints on size and mass than by the operational physics. Devices with power approaching 100 GW would be conceivable if there were any applications that made the associated size, mass, and electrical requirements tolerable.

The bulk of the work in this area has concentrated on oscillators. Prevention of oscillations is very difficult in such high power devices with the transients that accompany the pulsed power producing the beams. Nevertheless, high power TWT amplifiers have been explored, and power levels as high as 1 GW have been reached, although this latter system was plagued by a tendency to go into oscillation as the beam radius expanded over the course of a pulse.

Problems

1. Some slow-wave structures have a sinusoidally rippled wall with a wall radius described by Equation 8.8:

$$r_w(z) = r_0 + r_1 \sin(h_0 z)$$

with $h_0 = 2\pi/z_0$. Plot $r_w(z)$ over the range $0 \le z \le 3z_0$ for $r_0 = 1.5$ cm, $r_1 = 0.15$ cm, and $z_0 = 1.1$ cm.

2. We can approximate the dispersion curve (ω vs. k_z) for a slow-wave structure by using the dispersion curves for the TM_{0p} modes of a smooth-walled waveguide over the appropriate values of k_z. Before we turn to the slow-wave-structure dispersion curves, consider the dispersion curves for the TM_{0p} modes of a cylindrical waveguide of constant radius r_0. The dispersion curves for the smooth-walled waveguide are given by Equation 8.4:

$$\omega^2 = k_n^2 c^2 + \omega_{co}^2(0,p)$$

where, according to Equation 8.5,

$$\omega_{co}(0,p) = \frac{\mu_{op} c}{r_0}$$

with the μ_{0p} solutions to the equation

$$J_0(\mu_{0p}) = 0$$

and

$$k_n = k_z + nh_0$$

a. What are the four smallest values of μ_{0p}?

b. For a waveguide radius of $r_0 = 1.5$ cm, what are the four lowest cutoff frequencies, $f_{co} = \omega_{co}/2\pi$, for the four lowest-frequency TM_{0p} modes of the waveguide?

c. Plot the dispersion relation of Equation 8.4 for the four lowest-frequency TM_{0p} modes for k_z in the range

$$-\frac{3\omega_{co}(0,1)}{c} \le k_z \le \frac{3\omega_{co}(0,1)}{c}$$

d. Just so we recognize the TE_{0p} smooth-walled-waveguide modes if we ever come across them in an experiment, we note that their dispersion relation has the same form as the TM_{0p} modes, except that the cutoff frequencies for these modes are given by the following, with μ_{0p} replaced by ν_{0p}, which are the solutions to

$$J_0'(\nu_{0p}) = 0$$

For our 1.5-cm-radius smooth-walled waveguide, what are the four lowest cutoff frequencies, $f_{co} = \omega_{co}/2\pi$, for the four lowest-frequency TE_{0p} modes of the waveguide?

e. Return to the TM_{0p} modes again. What is the frequency in GHz, $f = \omega/2\pi$, of the TM_{01} mode for $k_z = \omega_{co}/c$? What is the wavelength in centimeters in free space of the wave at that frequency? Within the waveguide, what is the wavelength along the axis for that same wave?

3. Consider a slow-wave structure with a sinusoidally rippled wall described by Equation 8.8, with $r_0 = 1.75$ cm, $r_1 = 0.1$ cm, and $z_0 = 1.2$ cm. Sketch, or plot using your computer, the three space harmonics, for n = –1, 0, and 1 in the expression for k_n, for the lowest three TM_{0p} modes of a smooth-walled waveguide with radius r_0 for k_z between $-3h_0/2$ and $3h_0/2$. Now sketch in the form of the slow-wave-structure dispersion curves for that range of k_z using the procedure outlined in Section 4.4.1.

Each mode of the slow-wave structure has its own continuous dispersion curve. Because the lowest-frequency mode of the SWS is well approximated by space harmonics of the smooth-wall-waveguide TM_{01} mode, we sometimes call it the TM_{01}-like mode, or even the TM_{01} mode, although we have to be careful what we mean when we use the latter shorthand. The dispersion curve for each mode extends over a range of frequencies known as its passband. Sometimes passbands overlap, even though the SWS dispersion curves do not intersect or cross.

a. What is the approximate value of the lowest frequency in the passband of the lowest-order, TM_{01}-like mode of the slow-wave structure? What are the wavenumbers for which the frequency has this value?

b. What is the approximate value of the highest frequency in the passband of the lowest-order, TM_{01}-like mode of the slow-wave structure? What are the wavenumbers for which the frequency has this value?

c. What is the range of frequencies over which the passband extends for the next-higher-order mode? What are the wavenumbers at the lowest and highest frequencies in the passband?

d. In the second-lowest-order passband of part (c), over what range of wavenumbers will the mode have the character of a TM_{01} mode of a smooth-wall waveguide? Over what range of wavenumbers will it have the character of a TM_{02} mode of a smooth-wall waveguide?

e. Would you expect that the TM_{01}-like mode would permit operation as a surface wave oscillator? Check against Equation 8.9.

4. Return to the slow-wave structure of Problem 3 and the dispersion curves we sketched for it. Now we will include a beam in the problem.

a. What velocity would a beam have to have in order for its associated beam line, $\omega = k_z v_b$, to intersect the dispersion curve of the second-lowest-order mode (i.e., the next one up from the TM_{01}-like mode) at the 2π point? The 2π point is where the wavenumber is such that $k_z z_0 = 2\pi$. A mode with this wavenumber goes through a phase shift of 2π for each section of the slow-wave structure.

b. At what values of ω and k_z does a beam line for a beam of the velocity you found in part (a) intersect the lowest, TM_{01}-like mode of the slow-wave structure?

5. The peak of the lowest mode of the slow-wave structure at $k_z = h_0/2$ is located near the intersection of the n = 0 and n = –1 space harmonics of the smooth-walled-waveguide TM_{01} dispersion curve. However, it is pushed down from that intersection by the formation of a gap between the lowest and the second-lowest dispersion curves for the slow-wave structure. That gap gets larger, and the peak of the dispersion curve is pushed downward, as the ripple, or the perturbation, in the wall of the slow-wave structure increases in size (e.g., as the ratio of r_1/r_0, terms given in Equation 8.9, gets larger).

a. For a slow-wave structure with the dimensions given in Problem 3 ($r_0 = 1.75$ cm, $r_1 = 0.1$ cm, and $z_0 = 1.2$ cm) and a beam with axial velocity $v_b = 2 \times 10^{10}$ cm/sec, how low does the peak frequency for the lowest TM_{01}-like slow-wave-structure mode have to be if the beam line is to intersect that curve at its peak, as in a surface wave oscillator?

b. What is the electron kinetic energy, $(\gamma_b - 1)mc^2$, measured in electron volts?

6. In this chapter, most of our discussion of the addition of an electron beam to the slow-wave structure has used the beam line approximation,

$$\omega = k_z v_b$$

in which we ignore the fact that there are actually two space-charge waves on the beam — which we can see clearly in Figure 8.7 — and ignore the frequency splitting between them. With more accuracy (but less than if we solved the complete dispersion relation in the references), it is customary to approximate the dispersion relation for the slow space-charge wave by

$$\omega = k_z v_b - \omega_q$$

where ω_q is an effective plasma frequency for a beam in a waveguide or SWS. Just as it is a reasonable approximation to ignore the effect of the beam in estimating the dispersion curves for the slow-wave structure, we can estimate the slow space-charge wave dispersion by ignoring the SWS and computing the dispersion curves for a beam in a smooth-walled waveguide.

Find the dispersion relation for the space-charge waves for a thin beam of radius r_b, current I_b, and electron kinetic energy $(\gamma_b - 1)mc^2$ in a waveguide of radius r_0 with perfectly conducting walls. Assume that (1) the beam is guided by a large enough magnetic field that electron motions are only axial along z, (2) all quantities are independent of the azimuthal variable θ and depend on z and t as $\exp[i(k_z z - \omega t)]$, and (3) the electromagnetic fields are transverse magnetic TM_{0p} waves with only E_r, E_z, and B_θ components. Further, assume that beam quantities can be written as a large zero-order piece plus perturbations created by the beam; for example, the electron velocity can be written as $v_b = v_{b0} + v_{b1}$, with $v_{b0} >> v_{b1}$. Therefore, ignore all products of the small perturbations.

a. First derive the form of the electric and magnetic fields both inside the beam, $0 \le r < r_b$, and outside the beam, $r_b < r < r_0$. Choose the solutions for which the fields are bounded on the axis and obey the boundary condition at the perfectly conducting waveguide wall.

b. Use Newton's law (F = ma) and Maxwell's equations to relate the perturbations to the beam quantities v_{b1}, γ_{b1}, and n_{b1} (density) to the fields of part (a).

c. Match the electric and magnetic fields across the beam, taking account of discontinuities in the azimuthal magnetic field and the radial electric field at the beam. Hint: Because the beam is thin, you only have to integrate the current density across it:

$$\int_{r_b-\varepsilon}^{r_b+\varepsilon} j_b 2\pi r dr = I_b$$

where j_b is the current density in the beam.

d. The resulting expression is your dispersion relation. It must be solved numerically to find ω vs. k_z, and the solutions will include the space-charge waves as well as electromagnetic waveguide modes. The space-charge modes will have dispersion relations straddling the beam line. The term ω_q in our earlier expression can be found numerically as a function of the beam parameters and k_z.

7. Using Equation 8.14 and the information in Figure 8.13, for a fixed beam–wall standoff of 5 mm (i.e., $r_0 - r_b = 5$ mm), plot the maximum power that an electron beam can provide as a function of wall radius r_0 in a smooth-walled waveguide for voltages V of (a) 500 kV, (b) 1 MV, and (c) 1.5 MV. Also, for each voltage, plot the beam current I_b and the impedance (V/I_b) vs. r_0. Remember that many of these devices operate at an impedance of about 100 Ω.

8. In this problem, we will scope out some of the major parameters of a large-diameter MWCG. We start by fixing the following design parameters:

- Voltage V = 2 MV
- Linear beam current density $I_b/2\pi r_b = 0.4$ kA/cm
- Ratio of diameter $D = 2r_0$ to free-space wavelength λ, $D/\lambda = 10$
- Frequency $f = \omega/2\pi = 10$ GHz
- Magnetic field B = 2 T

a. Compute the beam velocity, v_b, neglecting any loss of beam energy to space-charge effects in the slow-wave structure (i.e., simply use the voltage to compute γ_b). We need this for our beam line.

b. An MWCG operates at the peak of the lowest-frequency, TM_{01}-like passband in the π-mode. Find the value of the slow-wave-structure period z_0 that allows for a resonance with the beam line at the peak. Remember that this is an approximate calculation and that the exact value would depend on a full solution of the dispersion relation. How far in frequency below the intersection of the n = 0 and n = –1 space harmonics of the smooth-walled-waveguide TM_{01} modes does the peak of the SWS curve have to lie?

c. If the beam spacing from the average wall radius, $r_0 - r_b$, is to be 6 mm, what is the beam current, given the fixed value of linear

beam current density? What is the impedance, V/I_b? Is this value of beam current allowed by Equation 8.14?

d. Given the radius of the SWS, assuming that the field coils producing the guide field are placed up against the structure, what is the energy per unit length of SWS stored in the magnetic field, which has energy density $B^2/2\mu_0$?

9. Consider a 100-Ω BWO driven by a pulsed power generator with an output impedance of 50 Ω. The voltage at the BWO is 1 MV, and the BWO generates microwaves with 25% efficiency.

   a. What is the output power of this device?

   b. What voltage at the pulsed power generator, V_{PP}, is required to provide 1 MV at the BWO?

   c. While we make much of source efficiency, the ratio of microwave output power to the electron beam power, system efficiencies are important as well. What is the system efficiency from pulsed power to microwave output? To be specific, what is the ratio of microwave power output to pulsed power input?

10. Dielectric Cerenkov masers (DCMs) use smooth-wall waveguides with dielectric liners to reduce the phase velocity of the normal electromagnetic modes of the structure so they can interact with the beam electrons.

    a. Compute the cutoff frequency of the TM_{01} mode, in both radians/sec and Hz, for a cylindrical waveguide with perfectly conducting walls of radius 4 cm.

    b. Now, assume a dielectric liner with relative permittivity $\varepsilon = 2$ fills the inside of the waveguide of part (a) between $r = 2$ cm and the wall. Derive a dispersion relation between ω and k_z for this modified waveguide. Show that the form of the dispersion relation will be the same as for the waveguide without the dielectric linear, albeit with a modified cutoff frequency for each mode.

    c. The dispersion relation in part (b) will require a numerical solution. Without determining the actual value of the cutoff frequency for the TM_{01} mode, we can denote it ω_{co}. Derive an expression for the resonant frequency at which the beam line for a beam of energy γ_0 intersects the dispersion curve for the dielectric-lined waveguide.

References

1. Kompfner, R., The invention of traveling wave tubes, *IEEE Trans. Electron Dev.*, ED-23, 730, 1976.

2. Nation, J.A., On the coupling of a high-current relativistic electron beam to a slow wave structure, *Appl. Phys. Lett.*, 17, 491, 1970.
3. Kovalev, N.F. et al., Generation of powerful electromagnetic radiation pulses by a beam of relativistic electrons, *JETP Lett.*, 18, 138, 1973 (*ZhETF Pis. Red.*, 18, 232, 1973).
4. Bogdankevich, L.S., Kuzelev, M.V., and Rukhadze, A.A., Plasma microwave electronics, *Sov. Phys. Usp.*, 24, 1, 1981 (*Usp. Fiz. Nauk*, 133, 3, 1981).
5. Carmel, Y. et al., Intense coherent Cerenkov radiation due to the interaction of a relativistic electron beam with a slow-wave structure, *Phys. Rev. Lett.*, 33, 1278, 1974.
6. Aleksandrov, A.F. et al., Excitation of surface waves by a relativistic electron beam in an irised waveguide, *Sov. Phys. Tech. Phys.*, 26, 997, 1981 (*Zh. Tekh. Fiz.*, 51, 1727, 1981).
7. Aleksandrov, A.F. et al., Relativistic source of millimeter-wave diffraction radiation, *Sov. Tech. Phys. Lett.*, 7, 250, 1981 (*Pis'ma Zh. Tekh. Fiz.*, 7, 587, 1981).
8. The *orotron* is similar to an RDG; see Bratman, V.L. et al., The relativistic orotron: a high-power source of coherent millimeter microwaves, *Sov. Tech. Phys. Lett.*, 10, 339, 1984 (*Pis'ma Zh. Tekh. Fiz.*, 10, 807, 1984).
9. Bugaev, S.P. et al., Relativistic multiwave Cerenkov generator, *Sov. Tech. Phys. Lett.*, 9, 596, 1983 (*Pis'ma Zh. Tekh. Fiz.*, 9, 1385, 1983).
10. Bugaev, S.P. et al., Relativistic bulk-wave source with electronic mode selection, *Sov. Tech. Phys. Lett.*, 10, 519, 1984 (*Pis'ma Zh. Tekh. Fiz.*, 10, 1229, 1984).
11. Bastrikov, A.N. et al., "GAMMA" high-current electron accelerator, *Instrum. Exp. Tech.*, 32, 287, 1989 (*Prib. Tekh. Eksp.*, 2, 36, 1989).
12. Bugaev, S.P. et al., Interaction of an electron beam and an electromagnetic field in a multiwave 10^{10} W Cerenkov generator, *Sov. J. Commun. Tech. Electron.*, 32, 79, 1987 (*Radiotekh. Elektron.*, 7, 1488, 1987).
13. Bugaev, S.P. et al., Relativistic multiwave Cerenkov generators, *IEEE Trans. Plasma Sci.*, 18, 525, 1990.
14. Bugaev, S.P. et al., Investigation of a millimeter wavelength range relativistic diffraction generator, *IEEE Trans. Plasma Sci.*, 18, 518, 1990.
15. Korovin, S.D. et al., Relativistic backward wave tube with variable phase velocity, *Sov. Tech. Phys. Lett.*, 18, 265, 1992 (*Pis'ma Zh. Tekh. Fiz.*, 18, 63, 1992).
16. Korovin, S.D. et al., The effect of forward waves in the operation of a uniform relativistic backward wave tube, *Tech. Phys. Lett.*, 20, 5, 1994 (*Pis'ma Zh. Tekh. Fiz.*, 20, 12, 1994).
17. Moreland, L.D. et al., Enhanced frequency agility of high-power relativistic backward wave oscillators, *IEEE Trans. Plasma Sci.*, 24, 852, 1996.
18. Gunin, A.V. et al., Relativistic BWO with electron beam pre-modulation, in *Proceedings of the 12th International Conference on High-Power Particle Beams, BEAMS'98*, Haifa, Israel, 1998, p. 849.
19. Gunin, A.V. et al., Experimental studies of long-lifetime cold cathodes for high-power microwave oscillators, *IEEE Trans. Plasma Sci.*, 28, 537, 2000.
20. Bunkin, B.V. et al., Radar based on a microwave oscillator with a relativistic electron beam, *Sov. Tech. Phys. Lett.*, 18, 299, 1992.
21. Clunie, D. et al., The design, construction and testing of an experimental high power, short-pulse radar, in *Strong Microwaves in Plasmas*, Litvak, A.G., Ed., Russian Academy of Science, Institute of Applied Physics, Nizhny Novgorod, 1997, pp. 886–902.

22. Russia Locks Phasors and Boldly Goes …, *Asia Times* online, October 21, 2001, http://atimes.com/c-asia/CJ27Ag03.html.
23. Shiffler, D. et al., Gain and efficiency studies of a high power traveling wave tube amplifier, *Proc. SPIE*, 1226, 12, 1990.
24. Abubakirov, E.B. et al., An X-band gigawatt amplifier, *IEEE Trans. Plasma Sci.*, 30, 1041, 2002.
25. Butler, J.M. and Wharton, C.B., Twin traveling-wave tube amplifiers driven by a relativistic backward-wave oscillator, *IEEE Trans. Plasma Sci.*, 24, 884, 1996.
26. Main, W., Cherry, R., and Garate, E., High-power dielectric Cerenkov maser oscillator experiments, *IEEE Trans. Plasma Sci.*, 18, 507, 1990.
27. Didenko, A.N. et al., Cerenkov radiation of high-current relativistic electron beams, *Sov. Tech. Phys. Lett.*, 9, 26, 1983 (*Pis'ma Zh. Tekh. Fiz.*, 9, 60, 1983).
28. Walsh, J., Marshall, T., and Schlesinger, S., Generation of coherent Cerenkov radiation with an intense relativistic electron beam, *Phys. Fluids*, 20, 709, 1977.
29. Kuzelev, M.V. et al., Relativistic high-current plasma microwave electronics: advantages, progress, and outlook, *Sov. J. Plasma Phys.*, 13, 793, 1987 (*Fiz. Plazmy*, 13, 1370, 1987).
30. Vlasov, A.N. et al., Overmoded GW-class surface-wave microwave oscillator, *IEEE Trans. Plasma Sci.*, 28, 550, 2000.
31. Kurilko, V.I. et al., Stability of a relativistic electron beam in a periodic cylindrical waveguide, *Sov. Phys. Tech. Phys.*, 24, 1451, 1979 (*Zh. Tekh. Fiz.*, 49, 2569, 1979).
32. Bromborsky, A. and Ruth, B., Calculation of TM_{on} dispersion relations in a corrugated cylindrical waveguide, *IEEE Trans. Microwave Theory Tech.*, MTT-32, 600, 1984.
33. Swegle, J.A., Poukey, J.W., and Leifeste, G.T., Backward wave oscillators with rippled wall resonators: analytic theory and numerical simulation, *Phys. Fluids*, 28, 2882, 1985.
34. Guschina, I.Ya. and Pikunov, V.M., Numerical method of analyzing electromagnetic fields of periodic waveguides, *Sov. J. Commun. Tech. Electron.*, 37, 50, 1992 (*Radiotekh. Elektron.*, 8, 1422, 1992).
35. Swegle, J.A., Starting conditions for relativistic backward wave oscillators at low currents, *Phys. Fluids*, 30, 1201, 1987.
36. Bugaev, S.P. et al., Features of physical processes in relativistic diffraction oscillators near the 2π oscillation mode, *Sov. J. Commun. Tech. Electron.*, 35, 115, 1990 (*Radiotekh. Elektron.*, 7, 1518, 1990).
37. Miller, S.M. et al., Theory of relativistic backward wave oscillators operating near cutoff, *Phys. Plasmas*, 1, 730, 1994.
38. Abubakirov, E.B. et al., Cyclotron-resonance mode selection in Cerenkov relativistic-electron RF sources, *Sov. Tech. Phys. Lett.*, 9, 230, 1983 (*Pis'ma Zh. Tekh. Fiz.*, 9, 533, 1983).
39. Bratman, V.L. et al., Millimeter-wave HF relativistic electron oscillators, *IEEE Trans. Plasma Sci.*, 15, 2, 1987.
40. Ginzburg, N.S., Kuznetsov, S.P., and Fedoseeva, T.N., Theory of transients in relativistic backward-wave tubes, *Radiophys. Quantum Electron.*, 21, 728, 1978 (*Izv. VUZ Radiofiz.*, 21, 1037, 1978).
41. Belov, N.E. et al., Relativistic carcinotron with a high space charge, *Sov. J. Plasma Phys.*, 9, 454, 1983 (*Fiz. Plazmy*, 9, 785, 1983).
42. Levush, B. et al., Theory of relativistic backward wave oscillators with end reflections, *IEEE Trans. Plasma Sci.*, 20, 263, 1992.
43. Levush, B. et al., Relativistic backward-wave oscillators: theory and experiment, *Phys. Fluids B*, 4, 2293, 1992.
44. Vlasov, A. et al., Relativistic backward-wave oscillators operating near cyclotron resonance, *Phys. Fluids B*, 5, 1625, 1993.
45. Hegeler, F. et al., Studies of relativistic backward-wave oscillator operation in the cross-excitation regime, *IEEE Trans. Plasma Sci.*, 28, 567, 2000.
46. Vlasov, A.N., Nusinovich, G.S., and Levush, B., Effect of the zero spatial harmonic in a slow electromagnetic wave on operation of relativistic backward-wave oscillators, *Phys. Plasmas*, 4, 1402, 1997.
47. Bugaev, S.P. et al., Investigation of a multiwave Cerenkov millimeter-wave oscillator producing gigawatt power levels, *Sov. J. Commun. Tech. Electron.*, 34, 119, 1989 (*Radiotekh. Elektron.*, 2, 400, 1989).
48. Koshelev, V.I. and Deichuly, M.P., Optimization of electron beam-electromagnetic field interaction in multiwave Cerenkov generators, in *High Energy Density Microwaves*, Conference Proceedings 474, Phillips, R.M., Ed., American Institute of Physics, New York, 1999, p. 347.
49. Bugaev, S.P. et al., Atmospheric microwave discharge and study of the coherence of radiation from a multiwave Cerenkov oscillator, *Sov. Phys. Dokl.*, 32, 78, 1988 (*Dokl. Akad. Nauk SSSR*, 298, 92, 1988).
50. Bugaev, S.P. et al., Generation of intense pulses of electromagnetic radiation by relativistic high-current electron beams of microsecond duration, *Sov. Phys. Dokl.*, 29, 471, 1984 (*Dokl. Akad. Nauk SSSR*, 276, 1102, 1984).
51. Bastrikov, A.N. et al., The state of art of investigations of relativistic multiwave microwave generators, in *Proceedings of the 9th International Conference on High-Power Particle Beams, BEAMS'92*, Washington, D.C., 1992, p. 1586.
52. Korovin, S.D. and Rostov, V.V., High-current nanosecond pulse-periodic electron accelerators utilizing a Tesla transformer, *Russian Phys. J.*, 39, 1177, 1996.
53. Data provided during a tour of the Institute of High-Current Electronics, Tomsk.
54. Zagulov, F.Ya. et al., Pulsed high-current nanosecond electron accelerator with pulsing frequency of up to 100 Hz, *Instrum. Exp. Tech.*, 19, 1267, 1976.
55. El'chaninov, A.S. et al., Stability of operation of vacuum diodes of high-current relativistic electron accelerators, *Sov. Phys. Tech. Phys.*, 26, 601, 1981.
56. Bykov, N.M. et al., High-current periodic-pulse electron accelerator with highly stable electron-beam parameters, *Instrum. Exp. Tech.*, 32, 33, 1987.
57. Chen, C. et al., A repetitive X-band relativistic backward-wave oscillator, *IEEE Trans. Plasma Sci.*, 30, 1108, 2002.
58. Bugaev, S.P. et al., Surface sterilization using low-energy nanosecond pulsed electron beams, in *Proceedings of the 10th International Conference on High-Power Particle Beams, BEAMS'94*, San Diego, CA, 1994, p. 817. The accelerator in this paper is referred to as SINUS-13 in Korovin and Rostov.[52]
59. Luybutin, S.K. et al., Nanosecond hybrid modulator for the fast-repetitive driving of X-band, gigawatt-power microwave source, *IEEE Trans. Plasma Sci.*, 33, 1220, 2005.
60. Korovin, S.D. et al., Repetitive nanosecond high-voltage generator based on spiral forming line, 28th International Conference on Plasma Science and 13th IEEE Pulsed Power Conference, *Digest of Papers*, 1249, 2001.
61. Gorbachev, K.V. et al., High-power microwave pulses generated by a resonance relativistic backward wave oscillator with a power supply system based on explosive magnetocumulative generators, *Tech. Phys. Lett.*, 31, 775, 2005 (*Pis'ma Zh. Tekh. Fiz.*, 31, 22, 2005).

62. Belousov, V.I. et al., Intense microwave emission from periodic relativistic electron bunches, *Sov. Tech. Phys. Lett.*, 4, 584, 1978 (*Pis'ma Zh. Tekh. Fiz.*, 4, 1443, 1978).
63. Gunin, A.V. et al., Relativistic X-band BWO with 3-GW output power, *IEEE Trans. Plasma Sci.*, 26, 326, 1998.
64. Kitsanov, S.A. et al., Pulsed 5-GW resonance relativistic BWT for a decimeter wavelength range, *Tech. Phys. Lett.*, 29, 259, 2003 (*Pis'ma Zh. Tekh. Fiz.*, 29, 87, 2003).
65. Shiffler, D. et al., A high-power two stage traveling-wave tube amplifier, *J. Appl. Phys.*, 70, 106, 1991; Shiffler, D. et al., Sideband development in a high-power traveling-wave tube microwave amplifier, *Appl. Phys. Lett.*, 58, 899, 1991.
66. Kovalev, N.F. et al., Parasitic currents in magnetically insulated high-current diodes, *Sov. Tech. Phys. Lett.*, 3, 168, 1977 (*Pis'ma Zh. Tekh. Fiz.*, 3, 413, 1977).
67. Aleksandrov, A.F. et al., Broadening of a relativistic electron beam in Cerenkov-radiation source, *Sov. Tech. Phys. Lett.*, 14, 349, 1988 (*Pis'ma Zh. Tekh. Fiz.*, 14, 783, 1988).
68. Burtsev, V.A. et al., Generation of microsecond microwave pulses by relativistic electron beams, *Sov. Tech. Phys. Lett.*, 9, 617, 1983 (*Pis'ma Zh. Tekh. Fiz.*, 9, 1435, 1983).
69. Hahn, K., Fuks, M.I., and Schamiloglu, E., Initial studies of a long-pulse relativistic backward-wave oscillator using a disk cathode, *IEEE Trans. Plasma Sci.*, 30, 1112, 2002.
70. Korovin, S.D. et al., Pulsewidth limitation in the relativistic backward wave oscillator, *IEEE Trans. Plasma Sci.*, 28, 485, 2000.
71. Bugaev, S.P. et al., Collapse of a relativistic high-current electron beam during generation of high-power electromagnetic radiation pulses, *Radio Eng. Electron. Phys.*, 29, 132, 1984 (*Radiotekh. Elektron.*, 29, 557, 1984).
72. Korovin, S.D., Rostov, V.V., and Totmeninov, E.M., Studies of relativistic backward wave oscillator with low magnetic field, in *Proceedings of the 3rd IEEE International Vacuum Electronics Conference*, Monterey, CA, 2002, p. 53.
73. El'chaninov, A.S. et al., Highly efficient relativistic backward-wave tube, *Sov. Tech. Phys. Lett.*, 6, 191, 1980 (*Pis'ma Zh. Tekh. Fiz.*, 6, 443, 1980).
74. Tkach, Yu.V. et al., Microwave emission in the interaction of a high-current relativistic electron beam with a plasma-filled slow-wave structure, *Sov. J. Plasma Phys.*, 1, 43, 1975 (*Fiz. Plazmy*, 1, 81, 1975).
75. Carmel, Y. et al., Demonstration of efficiency enhancement in a high-power backward-wave oscillator by plasma injection, *Phys. Rev. Lett.*, 62, 2389, 1989.
76. Goebel, D.M., Schumacher, R.W., and Eisenhart, R.L., Performance and pulse shortening effects in a 200-kV PASOTRON HPM source, *IEEE Trans. Plasma Sci.*, 26, 354, 1998.

9

Klystrons and Reltrons

9.1 Introduction

The distinctive feature of *klystrons* and *reltrons* is that the microwave-generating interactions in these devices take place in resonant cavities at discrete locations along the beam. The drift tube connecting the cavities is designed so that electromagnetic wave propagation between the cavities is cut off; without electromagnetic coupling between cavities, they are coupled only by the bunched beam, which drifts from one cavity to the next. To guide the beam along the drift tube, an axial magnetic guide field is applied, so that klystrons and reltrons (in those instances where a magnetic field is applied) are O-type devices. By contrast, in other O-type devices, such as the Cerenkov sources, free-electron lasers, or gyro-devices, microwaves are generated by beam-wave resonances that transfer beam energy to a wave over an extended interaction space or in a series of electromagnetically coupled cavities. The attractions of klystrons are their high power and efficiency, potentially wide bandwidth, and phase and amplitude stability.

All of the truly high power klystrons are relativistic, with beam voltages of the order of 500 kV or higher. As we show in Figure 9.1, though, relativistic klystrons are clearly differentiated into two groups on the basis of the beam impedance and, as we shall see, the bunching mechanisms that accompany low- and high-impedance operation. *High-impedance klystrons*, with impedances of the order of 1 kΩ, operate much the same way as conventional klystrons, albeit at higher voltages. In most cases, high power klystrons in this class have been developed as drivers for the radio frequency linear accelerators (RF linacs) in high-energy electron-positron colliders. There are two subclasses of high-impedance klystrons: those that operate at mildly relativistic voltages near 500 kV and those that operate at fully relativistic voltages of 1 MV or more. *Low-impedance klystrons* with impedances of about 100 Ω or less, on the other hand, feature much higher space-charge forces, which provide for a uniquely powerful bunching mechanism.

The *reltron* is similar to klystrons in that microwave power is extracted from a bunched beam using a set of output cavities; however, it is unique